

Show Me What and Where has Changed?

Question Answering and Grounding for Remote Sensing Change Detection

Ke Li¹, Fuyu Dong¹, Di Wang^{1*}, Shaofeng Li^{1*}, Quan Wang¹, Xinbo Gao^{1,2}, Tat-Seng Chua³
¹ Xidian University, ² Chongqing University of Posts and Telecommunications,
³ National University of Singapore
<https://like413.github.io/CDQAG/>

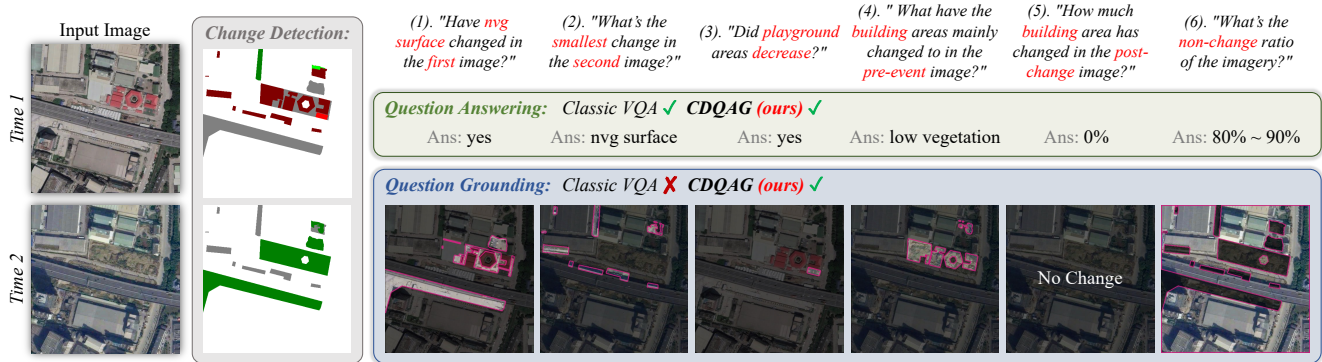


Figure 1. Change detection (CD) identifies surface changes from multi-temporal images. Classic visual question answering (VQA) only supports textual answers. In comparison, the proposed **change detection question answering and grounding (CDQAG)** supports well-founded answers, *i.e.*, textual answers (“*what has changed*”) and relevant visual feedback (“*where has changed*”).

Abstract

Remote sensing change detection aims to perceive changes occurring on the Earth’s surface from remote sensing data in different periods, and feed these changes back to humans. However, most existing methods only focus on detecting change regions, lacking the ability to interact with users to identify changes that the users expect. In this paper, we introduce a new task named **Change Detection Question Answering and Grounding (CDQAG)**, which extends the traditional change detection task by providing interpretable textual answers and intuitive visual evidence. To this end, we construct the first CDQAG benchmark dataset, termed **QAG-360K**, comprising over 360K triplets of questions, textual answers, and corresponding high-quality visual masks. It encompasses 10 essential land-cover categories and 8 comprehensive question types, which provides a large-scale and diverse dataset for remote sensing applications. Based on this, we present **VisTA**, a simple yet effective baseline method that unifies the tasks of question answering and grounding by delivering both visual and textual answers. Our method achieves state-of-the-art results on both the classic CDVQA and the proposed CDQAG datasets. Extensive qualitative and quantitative experimental results pro-

vide useful insights for the development of better CDQAG models, and we hope that our work can inspire further research in this important yet underexplored direction. The proposed benchmark dataset and method are available at <https://github.com/like413/VisTA>.

1. Introduction

Multi-temporal remote sensing imagery plays an essential role in the rapid acquisition of Earth’s surface change information, with applications across various fields such as environmental protection, resource management, and damage assessment [27, 32, 44]. However, existing remote sensing change detection systems primarily focus on full-picture analysis of coverage variations, such as binary segmentation and caption generation. Such systems lack the flexibility to accommodate human instructions [1, 42], thus constraining the advancement of user-friendly and effective remote sensing intelligent interpretation tasks.

Prior to this paper, several studies have attempted to enhance human-computer interaction in change detection tasks through natural language question answering (*e.g.*, CDVQA [41]). However, these methods neglect the intuitive visual explanations, *i.e.*, the change masks referred to by the complex questions, which fail to establish a link between textual answers and the corresponding vi-

*Corresponding author.

Datasets	Images	Questions	Textual-Ans.	Visual-Ans.
LEVIR-CD [2]	637	×	×	×
SECOND [37]	4,662	×	×	×
CDVQA [41]	2,968	122K	✓	×
QAG-360K	6,810	360K	✓	✓

Table 1. Comparison among different remote sensing change detection related datasets, including common segmentation datasets [2, 37], visual question answering dataset [41], and the proposed **QAG-360K**.

sual change regions. To this end, we first propose a novel task termed **Change Detection Question Answering and Grounding (CDQAG)**. As illustrated in Fig. 1, this task supports the simultaneous generation of textual answers and their associated pixel-level visual masks, providing an intuitive means for users to verify the answers and increasing their confidence in the reliability of the results. Therefore, exploring how to transcend the limitations of groundless answers and thoroughly investigate the semantic associations between the textual answers and visual groundings is of critical importance and constitutes the core research focus of this paper.

To propel the research of CDQAG, we construct the first benchmark dataset named QAG-360K, by extensively surveying, collecting, and standardizing 3 existing change detection datasets, generating 6,810 image pairs and over 360K high-quality $\{question, answer, mask\}$ triples through our automated data generation engine. Notably, the change queries include not only straightforward references (e.g., “playground”), but also more complicated description involving complex reasoning (e.g., “the land cover category with the smallest change” or “the area of land cover that increased”). Fig. 1 shows some examples of CDQAG task. For example, given “How much building area has changed in the post-change image?”, the output should provide both the proportion range of “building” and the corresponding change mask. Another example is “What is the smallest change in the second image?”, where the answer necessitates perceiving and evaluating changes across different categories to produce a correct textual-visual answer. Sec. 3 provides a comprehensive description and statistical analysis of the proposed dataset.

To accomplish this task, we develop a powerful benchmark framework called VisTA, which aims to tackle two key challenges: (1) How to reason about complex questions jointly with change images? (2) How to uncover the intrinsic relationships between the cross-modal answers? To solve the first challenge, the Multi-Stage Reasoning Module is designed to adaptively enhance cross-modal information interaction and fusion by jointly leveraging pixel-level visual representations and fine-granularity textual features. Notably, based on the observation that answer grounding typically depend on specific semantic cues in the question or answer, we introduce a question-answer selection mod-

ule to further refine the reasoning process. While the Text-Visual Answer Decoder is proposed to address the second challenge, which employs a text-to-pixel contrastive learning strategy to achieve fine-grained alignment between textual answers and visual masks.

In summary, our contributions are as follows:

- We propose a novel CDQAG task for remote sensing change detection. Unlike classic VQA (see Fig. 1), CDQAG not only generates textual answers but also provides pixel-level visual evidences, which is crucial for developing reliable remote sensing change detection systems.
- We construct the first CDQAG benchmark dataset QAG-360K, containing over 360K $\{question, answer, mask\}$ triples that are not only diverse but also contain comprehensive questions. This benchmark is essential for evaluation and encourages the community to further explore the CDQAG task.
- We present a solid CDQAG baseline method VisTA, which surpasses the latest visual question answering and visual grounding methods, achieving state-of-the-art performance on both the classic CDVQA and QAG-360K datasets.

2. Related work

Remote Sensing Change Detection. Remote sensing change detection involves identifying changes in land-cover information and plays a significant role in urban planning and environmental monitoring. By the type of change, it can be categorized into binary change detection [1, 5, 35] and semantic change detection [4, 30, 43]. The former only determines whether change have occurred between the two time periods, while the latter can further provide more detailed information about the categories of land-cover changes. Thus, we collect existing semantic change detection datasets [2, 29, 37], to prepare for CDQAG task.

Visual Question Answering. As a pivotal task in multimodal research, visual question answering (VQA) challenges models to respond to natural language queries based on images, making it a focal point in the domain of vision-language research. In recent years, the release of numerous benchmark datasets, including VQA [8], COCO-QA [24], Visual Genome [15], and CLEVR [13], has significantly accelerated progress in this field. Simultaneously, VQA also demonstrates its enormous potential in many applications such as education, healthcare, and remote sensing [11, 22, 33]. In particular, the introduction of CDVQA [41] has brought VQA into the domain of change detection, establishing a baseline dataset and method that expand the research frontiers of VQA while providing fresh perspectives for multimodal analysis in remote sensing.

Visual Grounding. Visual grounding (VG) focuses on localizing specific objects within images based on nat-

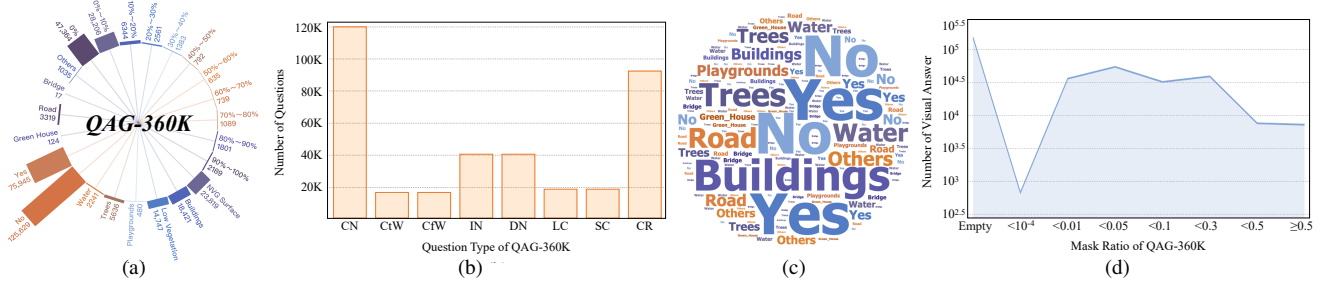


Figure 2. The proposed QAG-360K benchmark statistics: (a) the answer categories with frequency; (b) the distribution of question types (CN: change or not; CtW: change to what; CfW: change from what; IN: increase or not; DN: decrease or not; LC: largest change; SC: smallest change; CR: change ratio); (c) the word cloud of all questions; (d) the distribution of area ratio for visual masks.

ural language descriptions, and is typically divided into two subtasks: referring expression comprehension (REC) [3, 38, 40] and referring expression segmentation (RES) [36, 39]. REC aims to predict the bounding boxes of target objects from linguistic descriptions, while RES requires the generation of pixel-level segmentation masks of the referred targets. Recently, VG in remote sensing [17, 19] has gained increasing attention for its ability to intuitively highlight targets of interest against irrelevant backgrounds.

Question Answering and Grounding. As a hybrid task that combines VQA and VG, question answering and grounding (QAG) requires vision-language models to supply visual evidence while answering questions [9, 45]. Unlike traditional *post-hoc* interpretability methods [25, 26], QAG addresses concerns about “*whether answer reasoning is based on correct visual evidence*” by providing intuitive explanations, making it crucial for practical applications that require high safety and reliability. To support this capability, multiple VQA datasets now provide grounding labels such as VQS [7], GQA [12], and TVQA+ [16]. However, QAG remains largely unexplored in the field of remote sensing. To bridge this gap, we introduce CDQAG, the first benchmark dataset for the remote sensing change detection task, aiming to respond accurately and reliably to user inquiries about surface changes in different periods. The dataset comprises over 6.8K image pairs and 360K questions across 10 different land-cover categories. Compared with QAG tasks in natural scenes, remote sensing change detection involves more complex geospatial data and implicit reasoning relationships, imposing higher demands on the perception and interpretability capabilities of the models. Furthermore, existing visual responses are usually provided in the form of object-level bounding boxes [31, 45]. To meet the distinct requirements of change detection tasks, we provide pixel-level visual answers, enabling more precise and fine-grained analysis of changes.

3. Dataset Construction

We now introduce our task and dataset, which provide well-founded answers for land-cover change-related questions.

We first define the task of change detection visual question answering and grounding (CDQAG) and then present the first benchmark dataset QAG-360K.

3.1. Task Definition

The input of the CDQAG task contains a pair of remote sensing images T_1 and T_2 , captured in the same location but at a different time, along with a question Q . The output is a textual answer A and a corresponding visual segmentation S . Unlike classic VQA methods that provide only natural language responses, CDQAG can offer both textual answers and correlative visual explanations (as shown in Fig. 1), which is critical for reasonable remote sensing interpretation.

3.2. QAG-360K: A Large-scale CDQAG Dataset

To address the gap in this critical yet underexplored area, we introduce QAG-360K, the first benchmark dataset tailored for the CDQAG task. We collected a high-quality set of remote sensing images from existing binary and semantic change detection datasets, including Hi-UCD [29], SECOND [37], and LEVIR-CD [2]. These data cover 24 different regions across cities in Estonia, China and the United States, with spatial resolution ranging from 0.1 to 3.0 meters, providing diverse geographical scenarios. We filtered 6,810 remote sensing image pairs from these datasets as part of QAG-360K, including 10 land-cover categories, all of which are equipped with semantic masks. Additionally, we developed a specialized Triplet Generation Engine (in Appendix) to automatically produce change-related questions, textual answers, and corresponding visual masks.

Question Raised. To encompass a broad range of change scenarios, we expanded the change-related questions into **8C Questions**, covering the critical change detection types: *change or not? change to what? change from what? increase or not? decrease or not? largest change? smallest change? change ratio?* Moreover, to ensure that the phrasing of the questions conforms to natural communication, we utilized the Large Language Model (LLM) to generate an average of 20 question templates for each change type and then manually selected the most reasonable 5 for query-

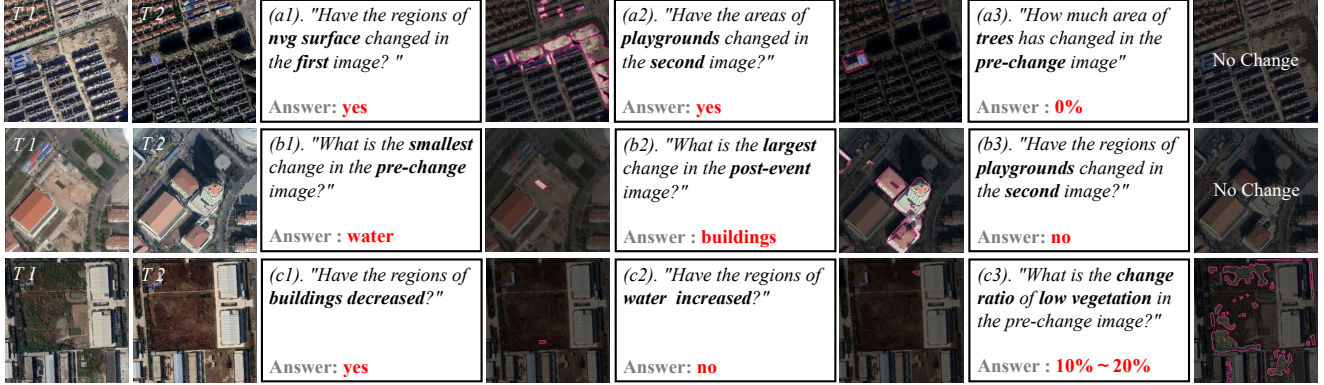


Figure 3. Examples of the proposed QAG-360K dataset.

ing. The final questions average 9.5 words in length, with lengths ranging from 4 to 15 words. Each pair of remote sensing images contains an average of 53 triples. Fig. 2b and Fig. 2c illustrate the distribution of all question types and the word clouds of land-cover categories, respectively. Detailed definitions and templates for each question type are provided in the Appendix.

Answers Generation. For each question type in the *8C Questions*, the answer generation follows different judgment rules. Specifically, existing change detection datasets offer mask annotations, which allow us to automatically generate textual answers and the corresponding pixel-level groundings based on predefined rules. The answer generation rules and specific procedures for each question type are detailed in the Appendix. Fig. 2d illustrates the distribution of mask area ratios for each visual answer. CDQAG introduces four critical and distinct attributes that are essential for practical applications:

- 1) **Temporal Semantic Correlation.** CDQAG involves comparing and analyzing multi-temporal remote sensing images. For instance, Fig. 3(a1) and Fig. 3(a2) pose two questions regarding pre-change and post-change conditions, respectively. The model is required to accurately discern and associate temporal semantic features from multi-temporal imagery, as dictated by natural language queries, in order to correctly evaluate and interpret changes in the target region.
- 2) **Complex and Implicit Reasoning.** In contrast to visual grounding tasks with clear-cut references, CDQAG typically involves complex reasoning about implicit information. For example, in Fig. 3(b1) and Fig. 3(b2), adjectives such as “largest” and “smallest” are used, requiring the model to match these descriptions to the corresponding areas. Furthermore, the QAG-360K dataset incorporates diverse ordinal expressions (*e.g.*, “before,” “pre-change,” and “first”) to indicate temporal changes, which necessitates that the model comprehend such terms to execute logical reasoning effectively.
- 3) **Fragmented Spatial Masks.** Unlike natural images,

which generally exhibit object-level semantic features, certain land-cover types in remote sensing imagery are spread across multiple regions, leading to fragmented and discontinuous segmentation masks. Fig. 3(c3) illustrates an example of proportional change in low vegetation. Moreover, when changes are extremely subtle, it poses a greater challenge for the model to accurately identify and segment them.

- 4) **Inconspicuous Visual Cues.** In certain instances, the query target may remain unchanged or may not appear at all, as exemplified by Fig. 3(a3) and Fig. 3(b2). Under such cases, the model must generate an empty mask to accurately indicate that no actual change has taken place, rather than resorting to guesswork. This imposes higher demands on the model’s reasoning capabilities, contextual comprehension, and capacity to handle uncertainty. These characteristics are pervasive throughout our dataset, ensuring that it maintains a balanced level of complexity. Furthermore, more examples from the QAG-360K dataset are provided in the Appendix.

4. Method

Next, we provide a detailed description of our proposed CDQAG model, VisTA, which delivers reliable textual answers and precise visual feedback. As shown in Fig. 4, our framework consists of three primary components, which are explained below.

4.1. Text and Image Feature Extraction

Text Encoder. Given a question $Q \in \mathbb{R}^L$, we leverage a CLIP pre-trained Transformer [23] to extract text features $F_t \in \mathbb{R}^{L \times C}$, where L denotes the question length and C represents the number of feature channels. The input text sequence is surrounded by two special tokens [SOS] and [EOC], where [EOC] is subsequently activated as a sentence-level representation $F_s \in \mathbb{R}^C$.

Image Encoder. For the two remote sensing images $T_1 \in \mathbb{R}^{H \times W \times 3}$ and $T_2 \in \mathbb{R}^{H \times W \times 3}$, we extract multi-scale visual features $F_{v_i}^1 \in \mathbb{R}^{H_i \times W_i \times C_i}$ and $F_{v_i}^2 \in \mathbb{R}^{H_i \times W_i \times C_i}$

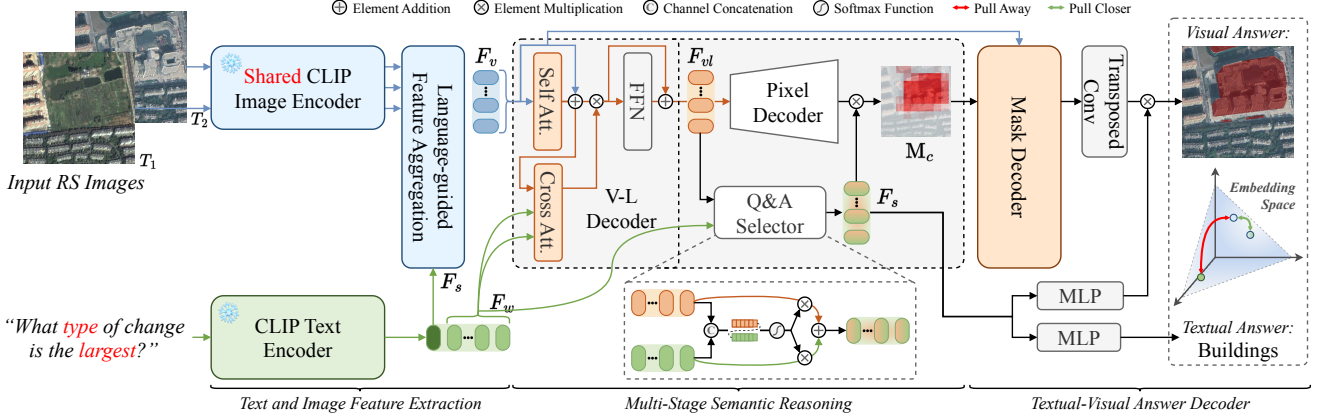


Figure 4. The architecture of our VisTA model as a simple baseline for the CDQAG task. Firstly, the given two remote sensing images and a question are encoded into vision features F_v and language features $[F_s, F_w]$, respectively. F_v and F_w are fed into a vision-language decoder to produce the refined multimodal features F_{vl} . Next, the Q&A selector is used to generate Q&A features F_s . Subsequently, F_s is activated as a selection weight to filter the pixel decoder’s output, resulting in coarse mask M_c . Finally, the textual-visual answer decoder is employed to predict the textual answer and the corresponding visual answer.

using two ResNets [10] with shared weights. Here, $i \in \{3, 4, 5\}$ denotes the i -th stage of visual backbone, and $H_i = H/2^i$ and $W_i = W/2^i$ are the corresponding resolutions. The original image dimensions are H and W , respectively. The ResNet is also pre-trained on CLIP, enhancing its visual representation capabilities. To obtain multi-scale change features $F_{c_i} \in \mathbb{R}^{H_i \times W_i \times C_i}$, we concatenate the visual features from both ResNets and utilize a 1×1 convolutional layer to adjust the channel dimensions:

$$F_{c_i} = \text{Conv}([F_{v_i}^1, F_{v_i}^2]), \quad (1)$$

where $[,]$ indicates concatenation.

Language-Guided Feature Aggregation. To efficiently fuse textual and change-related visual features, we design a module that initiates cross-modal feature fusion:

$$F_{m_5} = \text{Conv}(F_{c_5}) \cdot \text{Linear}(F_s), \quad (2)$$

where F_{m_5} represents the fused multi-modal features, and $\text{Linear}(\cdot)$ refers to a multi-layer perceptron that adjusts the dimensionality of the text features. We then feed F_{m_5} , F_{c_4} , and F_{c_3} into a common Feature Pyramid Network [18], denoted as $\mathcal{F}_{\text{FPN}}(\cdot)$, to extract multi-scale language-guided features:

$$F_{m_5}, F_{m_4}, F_{m_3} = \mathcal{F}_{\text{FPN}}(F_{m_5}, F_{c_4}, F_{c_3}). \quad (3)$$

Subsequently, we aggregate the three multi-modal features via a convolutional layer:

$$F_m = \text{Conv}([\text{Conv}(F_{m_5}), F_{m_4}, \text{DeConv}(F_{m_3})]), \quad (4)$$

where $\text{DeConv}(\cdot)$ signifies the deconvolutional layer. For subsequent cross-modal interaction, we flatten the output $F_m \in \mathbb{R}^{\frac{H}{16} \times \frac{W}{16} \times C}$ to obtain the preliminary visual features $F_v \in \mathbb{R}^{N \times C}$, where $N = H/16 \times W/16$.

4.2. Multi-Stage Semantic Reasoning

To address the complex reasoning demands of the CDQAG task, we propose a multi-stage reasoning module that facilitates fine-grained cross-modal information interaction. As shown in Fig. 4, given the pixel-level visual features F_v and word-level text features F_w , we construct a vision-language decoder to enable dense cross-modal interaction, producing a series of refined multi-modal features $F_{vl} \in \mathbb{R}^{N \times C}$. The interaction can be formalized as:

$$\begin{aligned} F'_v &= F_v + \text{SA}(F_v), \\ F'_{vl} &= \text{CA}(F'_v, F_w) \cdot F'_v, \\ F_{vl} &= \text{FFN}(F'_{vl} \cdot F'_v) + F'_{vl}, \end{aligned} \quad (5)$$

where $\text{SA}(\cdot)$ and $\text{CA}(\cdot)$ denote the multi-head self-attention and cross-attention layers, and $\text{FFN}(\cdot)$ refers to the feed-forward network. Since some questions or answers may lack explicit references, we introduce a Question and Answer Selector, allowing the model to dynamically select question-related or answer-related text representations. Rather than directly adding or concatenating these two features, we adaptively merge the multi-modal features F_{vl} and text features F_w via a soft attention mechanism, generating selection features F_s . This process can be expressed as:

$$\begin{aligned} \alpha &= \frac{e^{F_{vl}}}{e^{F_{vl}} + e^{F_w}}, \quad \beta = 1 - \alpha, \\ F_s &= \alpha F_{vl} + \beta F_w. \end{aligned} \quad (6)$$

We then activate F_s as a selection weight to filter out irrelevant change regions, which is formulated as:

$$M_c = \sigma(F_s) \otimes \mathcal{F}_{\text{PD}}(F_{vl}), \quad (7)$$

where $\sigma(\cdot)$ represents the sigmoid function, and $\mathcal{F}_{\text{PD}}(\cdot)$ is a pixel decoder that transforms F_{vl} into a coarse mask M_c .

4.3. Text-Visual Answer Decoder

We leverage the established visual coarse mask M_c and the question-answer features F_s for the final predictions. Specifically, in the visual branch, the coarse mask M_c serves as a dense visual prompt and is fed into the Mask Decoder $\mathcal{F}_{MD}(\cdot)$, along with original visual features F_v , to generate a more precise answer grounding:

$$\tilde{F}_M = \mathcal{F}_{MD}(M_c, F_v). \quad (8)$$

The Mask Decoder, comprising two consecutive Two-Way Attention Blocks [14], is designed to establish the pixel-level mapping between M_c and F_v . For textual answer, we apply a two-layer MLP followed by softmax activation to perform classification predictions. Notably, to enhance semantic consistency between visual and textual answers, we split and reshape the text features into a weight $W \in \mathbb{R}^{D \times K \times K}$ and a bias $b \in \mathbb{R}^D$, where K is the kernel size of the convolutional layer. This enables it to function as the kernel and bias for a 2D convolutional layer, transforming the visual features into the final precise binary mask M . The implementation can be formulated as follows:

$$\begin{aligned} W, b &= S\&R(\text{Linear}(F_s)), \\ M &= W * \tilde{F}_M + b, \end{aligned} \quad (9)$$

where $S\&R(\cdot)$ represents split and reshape, and $*$ is convolution operation.

4.4. Training Objective

Following prior works [20, 32], we employ the standard cross-entropy (CE) loss for textual answer classification and per-pixel binary cross-entropy (BCE) loss for visual answer prediction, denoted as \mathcal{L}_{txt} and \mathcal{L}_{mask} , respectively. It is noteworthy that we integrate a text-to-pixel contrastive loss into our training objective to enforce alignment between multimodal answers. Specifically, the text-to-pixel contrastive loss measures the similarity between the textual answer F_{ta} and the pixel-level visual answer F_{va} using a dot product. The contrastive loss \mathcal{L}_{con} is defined as:

$$\begin{aligned} \mathcal{L}_{con}(F_{ta}, F_{va}) &= \frac{1}{|\mathcal{P} \cup \mathcal{N}|} \sum_{i \in \mathcal{P} \cup \mathcal{N}} \mathcal{L}_{con}^i(F_{ta}, F_{va}^i), \\ s.t. \mathcal{L}_{con}^i(F_{ta}, F_{va}^i) &= \begin{cases} -\log \sigma(F_{ta} \cdot F_{va}^i), & i \in \mathcal{P}, \\ -\log(1 - \sigma(F_{ta} \cdot F_{va}^i)), & i \in \mathcal{N}, \end{cases} \end{aligned} \quad (10)$$

where \mathcal{P} and \mathcal{N} represent the positive and negative classes, respectively, in the ground truth. $|\mathcal{P} \cup \mathcal{N}|$ is the cardinality, and $\sigma(\cdot)$ is the sigmoid function. Our final objective function is:

$$\mathcal{L} = \lambda_1 \mathcal{L}_{txt} + \lambda_2 \mathcal{L}_{mask} + \lambda_3 \mathcal{L}_{con}, \quad (11)$$

where λ_1 , λ_2 , and λ_3 are hyperparameters that balance the three losses during training.

5. Experiments

5.1. Implementation Details

Datasets: We conduct extensive experiments on the proposed **QAG-360K** and classic **CDVQA** datasets. For **QAG-360K**, the distribution of the original data is heavily biased, so we remove some questions from the dataset, while intentionally retaining the original real-world tendencies up to a tunable degree. The advantage of this scheme is to make the benchmark more challenging and less biased. After that, we randomly split the dataset into 70% training, 10% validation, and 20% testing, making sure that all the questions about a given image appear in the same split. Besides, we use the **CDVQA** dataset to further validate the effectiveness of our method, which contains 2,968 image pairs, more than 120K question-answer pairs, and 6 land-cover categories.

Evaluation Metrics: Besides the widely-used VQA metrics average accuracy (AA) and overall accuracy (OA), we further introduce mean IoU (mIoU) and overall IoU (oIoU) for CDQAG. Detailed definitions of metrics can be found in the Appendix.

Configurations: We employ the CLIP pre-trained Transformer [23] and ResNet-101 [10] as the text and image encoders for all studies. The input image size and maximum sentence length are set to 512×512 pixels and 15 tokens, respectively. Each multi-head attention layer and feed-forward network uses default settings [6]. For the loss function in Eq. (11), we set $\lambda_1 = 0.2$ and $\lambda_2 = \lambda_3 = 1$. In the main results (Tab. 2), the second column represents each type in **8C Questions**: (CN: change or not; CtW: change to what; CfW: change from what; IN: increase or not; DN: decrease or not; LC: largest change; SC: smallest change; CR: change ratio). Following [34], we train the model for 50 epochs using the AdamW [21] optimizer with an initial learning rate of $1e-4$. The learning rate is decreased by a factor of 0.1 at the 35th epoch. We train the model with a batch size of 64 on 4 NVIDIA RTX4090 with 24 GPU VRAM. During inference, we binarize the predicted results using a threshold of 0.35 to obtain the final outputs.

Baseline Methods: Considering that existing methods rarely support both textual and visual answers, we add the same text or mask prediction heads as ours to RES models (e.g., CRIS [34], LAVT [39], CGFormer [28], and ETRIS [36]) and VQA models (e.g., RSVQA [20], CDVQA [41], and SOBA [33]). Moreover, since the aforementioned methods are not specifically designed for change detection, to ensure a fair comparison, we concatenate the two images and feed them into the visual backbone in the same way for all methods (except that marked with symbol †).

5.2. Comparisons with State-of-the-art Methods

Results on QAG-360K. In Tab. 2, we evaluate the performance of our proposed method in comparison with

Method		CRIS [34] CVPR'22	LAVT [39] CVPR'22	CGFormer [28] CVPR'23	ETRIS [36] ICCV'23	RSVQA [20] TGRS'21	CDVQA [41] TGRS'22	SOBA [33] AAAI'24	VisTA Ours	†VisTA Ours
Backbone		Res-101	Swin-B	Res-101	ViT-B/16	Res-101	ViT-B/16	Swin-T	Res-101	Res-101
Textual Answer	CN	82.29	83.43	82.90	84.08	81.73	82.30	84.74	<u>86.37</u>	87.02
	CtW	58.49	59.94	59.44	60.89	57.39	58.49	62.12	<u>66.48</u>	68.34
	CfW	58.57	59.37	59.46	60.22	57.60	60.34	60.95	<u>66.81</u>	69.92
	IN	79.59	81.66	81.02	82.39	75.28	76.02	81.08	<u>85.33</u>	87.05
	DN	80.32	81.08	81.44	82.99	78.18	77.66	80.69	<u>86.35</u>	87.43
	LC	52.16	52.81	53.52	55.25	47.89	49.19	56.91	<u>64.88</u>	68.08
	SC	31.76	32.52	32.35	33.11	29.81	28.91	33.87	<u>40.30</u>	41.57
	CR	66.87	69.00	68.45	69.50	63.73	61.81	69.76	<u>72.76</u>	74.79
	AA	63.76	64.98	64.82	66.06	61.45	62.46	66.27	<u>71.16</u>	73.03
	OA	69.50	70.89	70.58	71.78	67.35	68.60	71.98	<u>75.76</u>	77.35
b OA Decl.		-7.85	-6.46	-6.77	-5.57	-10.0	-8.75	-5.37	-1.59	-
Visual Answer	CN	21.70	24.82	23.05	28.50	13.84	14.96	26.92	<u>39.00</u>	44.18
	CtW	23.46	26.12	24.02	27.16	10.15	10.94	26.66	<u>33.84</u>	40.41
	CfW	27.68	30.32	27.93	31.57	10.76	11.97	31.10	<u>37.44</u>	43.30
	IN	28.66	30.71	27.62	33.56	17.40	17.61	32.68	<u>40.10</u>	45.74
	DN	25.97	29.00	26.47	30.56	17.70	18.61	29.88	<u>40.86</u>	46.55
	LC	36.44	37.53	36.85	39.66	17.27	18.11	38.88	<u>43.68</u>	48.71
	SC	9.89	14.94	10.52	17.88	1.39	1.76	16.92	<u>21.04</u>	24.78
	CR	54.98	58.46	56.17	59.57	46.84	47.31	58.86	<u>63.03</u>	65.86
	mIoU	28.60	31.49	29.08	33.56	16.91	17.66	32.74	<u>39.87</u>	44.94
	oIoU	37.42	40.28	38.83	42.56	28.54	29.33	41.83	<u>47.98</u>	52.13
b oIoU Decl.		-14.71	-11.85	-13.30	-9.57	-23.59	-22.80	-10.30	-4.15	-

Table 2. Comparisons with the state-of-the-art methods on the proposed **QAG-360K** test set. “b Decl.” indicates performance decline. The best and second best performance are highlighted in **bold** and underline. ‘†’ represents using two weight-shared visual backbone.

the state-of-the-art (SoTA) approaches on the QAG-360K test sets. Our method consistently outperforms competing methods in both the textual and visual answering tasks. Specifically, for classic textual answering, †VisTA achieves the highest AA of **73.03%** and OA of **77.35%**. Most importantly, it provides absolute improvements of up to **6.76%** on AA and **5.37%** on OA over the cutting-edge VQA method SOBA [33], demonstrating its superior ability to effectively capture intricate change-related relationships and perform complex reasoning. In the intuitive visual answering, our model also attains the best performance, achieving an mIoU of **82.6%** and an oIoU of **84.8%**. Compared to CRIS [34], CGFormer [28], and ETRIS [36], which also use ResNet-101, our method achieves improvements of **14.71%/13.30%/9.57%** on oIoU, respectively. †VisTA reaches an impressive performance **78.39%** on oIoU, reflecting a substantial advancement in comparison to the previous best method ETRIS (**13.25%/11.73%** for CtW/CfW). For the SC category, which requires finer spatial details, †VisTA achieves a **6.90%** improvement on oIoU over ETRIS. These performance gains highlight that our method can better model visual-language consistency, providing more precise and reliable visual evidence. Furthermore, compared to VisTA, the improved performance of †VisTA shows the advantages of dual shared-weight encoders in effectively extracting and aligning change-related information across scenes.

Results on CDVQA. We also compare our method with SoTA methods on the two CDVQA test subsets, as illus-

Method		RSVQA [20] TGRS'21	CDVQA [41] TGRS'22	SOBA [33] AAAI'24	Ours -
Test 1	AA	52.1	55.3	60.3	65.9
	OA	62.8 (-10.3)	65.9 (-7.2)	69.2 (-3.9)	73.1
Test 2	AA	52.2	55.4	60.3	65.9
	OA	57.9 (-10.6)	61.1 (-7.4)	64.8 (-3.7)	68.5

Table 3. Comparison with the state-of-the-art methods on the two **CDVQA** test sets. The best performance are highlighted in **bold**.

trated in Tab. 3. Our method consistently outperforms the baselines in both AA and OA metrics. Specifically, on Test 1, our method achieves an OA of **73.1%**, signifying a substantial improvement of **10.3%** over RSVQA, **7.2%** over CDVQA, and **3.9%** over SOBA. On Test 2, our approach maintains its advantage with an AA of **66.0%** and an OA of **69.5%**, further demonstrating significant improvements over existing SoTA approaches. These results underscore the robustness and generalization capabilities of our model, particularly in challenging VQA scenarios. More experimental results are presented in Appendix.

Qualitative results. As depicted in Fig. 5, our model accurately answers the change-related questions and provides intuitive and high-quality visual evidence. More visualizations are given in the Appendix. We also show some failure cases in Fig. 6. In the first row, although the prediction is correct and the visual evidence aligns well with the textual answer, the regions of buildings are discrete units in the ground-truth (GT), while our model generates continuous masks with overly smooth boundaries. This discrepancy underscores the difficulty of accurately capturing the discrete nature of certain objects. In the second case, the color of

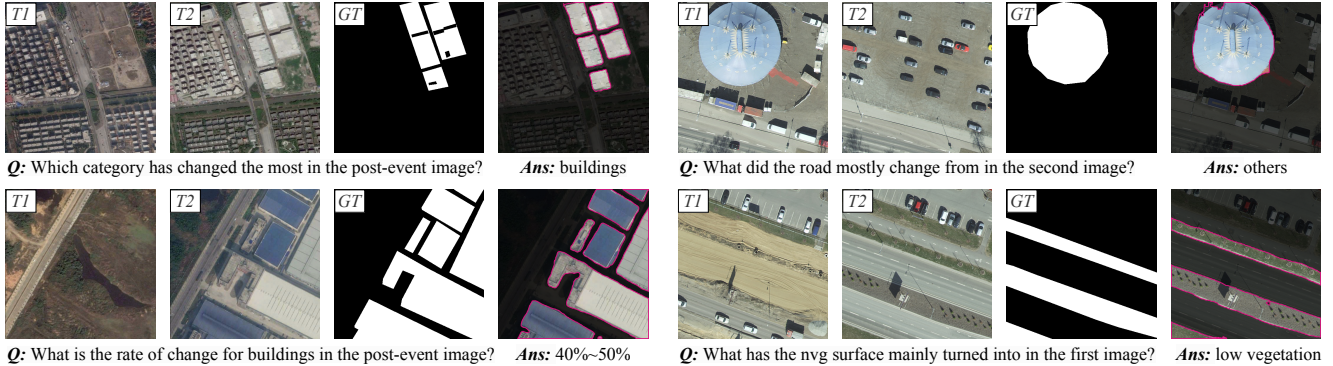


Figure 5. Example results of our method on QAG-360K dataset.

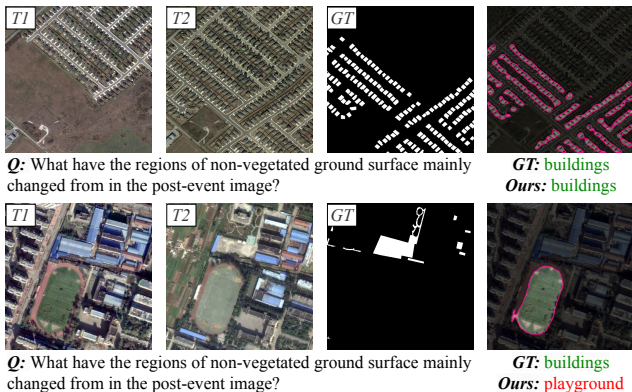


Figure 6. Failure cases of our method on QAG-360K dataset.

the playground fades over time, leading to the model mistakenly classify it as a “non-vegetated ground surface” that closely resembles the visual change, resulting in an incorrect prediction. This further requires models to perceive subtle visual cues and comprehend context-sensitive differences for more accurate visual answers.

5.3. Ablation Study

Effect of VisTA’s component. To validate the effectiveness of the proposed modules, we conduct ablation experiments on QAG-360K, which is summarized in Tab. 4. In the baseline model, the features extracted from visual and text encoders are concatenated and then input to the segmentation and classification heads, respectively. In Exp.2, language-guided feature aggregation (LGFA) is added onto the baseline model, which brings improvement of **1.61%** OA and **3.04%** oIoU. Exp.3 and Exp.4 further investigate the importance of multi-stage reasoning in CDQAG task, demonstrating the effectiveness of fine-grained semantic information interaction. Moreover, Exp.5 and Exp.6 highlight the benefit of auxiliary supervision via multimodal answer prediction, increasing the OA and oIoU of **4.90%** and **3.97%**.

Numbers of Layers in Vision-Language Decoder. The impact of the number of layers in visual-language decoder is shown in Fig. 7. When the visual representations are sequentially processed by more layers, the model consistently

Exp.	Methods	AA	OA	mIoU	oIoU
1	Baseline	62.58	68.29	28.73	37.51
2	Exp.1 + LGFA	64.48	69.90	31.11	40.55
3	Exp.2 + V-L Decoder	67.36	71.59	34.28	43.60
4	Exp.3 + Q&A Selector	69.77	73.88	37.90	46.02
5	w/o Textual Answering	58.21	70.86	-	-
6	w/o Visual Answering	-	-	35.66	44.01
7	VisTA (Ours)	71.16	75.76	39.87	47.98

Table 4. Effectiveness of the proposed components in VisTA.

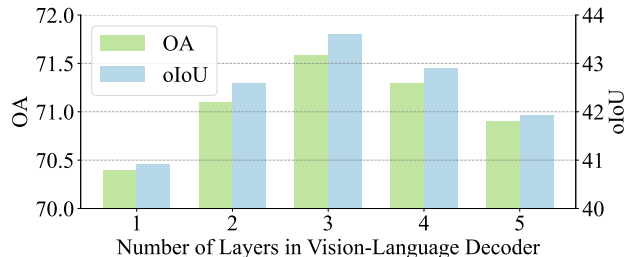


Figure 7. Effectiveness of the number of V-L Decoder’s layers.

achieves higher OA and oIoU. However, the setting of $n \geq 4$ introduces more parameters, which could increase the risk of over-fitting. Considering the performance and efficiency, we set $n = 3$ as the default in our framework.

6. Conclusions and Limitations

In this paper, we addressed key limitations of the classic CDVQA task, *i.e.*, its inability to simultaneously provide textual answers and corresponding visual evidence. To overcome this, we proposed the CDQAG benchmark, designed to offer intuitive visual explanations alongside textual answers. To facilitate research on CDQAG, we constructed the first large-scale dataset QAG-360K, and proposed an effective baseline method VisTA, which achieves the new SoTA performance on both our QAG-360K and CDVQA datasets. We hope that our work can shed new light on change detection. However, this study has two limitations: (1) The limited availability of public change detection datasets restricts the growth of this field. (2) While MLLMs show potential in complex reasoning, our work only establishes a baseline without an in-depth exploration of their performance. Future work could explore advanced

MLLM architectures for CDQAG, which may yield deeper insights and improved results.

References

- [1] Maximilian Bernhard, Niklas Strauß, and Matthias Schubert. Mapformer: Boosting change detection by using pre-change information. In *Proceedings of the IEEE/CVF International Conference on Computer Vision*, pages 16837–16846, 2023. 1, 2
- [2] Hao Chen and Zhenwei Shi. A spatial-temporal attention-based method and a new dataset for remote sensing image change detection. *Remote Sensing*, 12(10):1662, 2020. 2, 3
- [3] Jiajun Deng, Zhengyuan Yang, Daqing Liu, Tianlang Chen, Wengang Zhou, Yanyong Zhang, Houqiang Li, and Wanli Ouyang. Transvg++: End-to-end visual grounding with language conditioned vision transformer. *IEEE Transactions on Pattern Analysis and Machine Intelligence*, 2023. 3
- [4] Lei Ding, Jing Zhang, Haitao Guo, Kai Zhang, Bing Liu, and Lorenzo Bruzzone. Joint spatio-temporal modeling for semantic change detection in remote sensing images. *IEEE Transactions on Geoscience and Remote Sensing*, 2024. 2
- [5] Sijun Dong, Libo Wang, Bo Du, and Xiaoliang Meng. Changeclip: Remote sensing change detection with multi-modal vision-language representation learning. *ISPRS Journal of Photogrammetry and Remote Sensing*, 208:53–69, 2024. 2
- [6] Alexey Dosovitskiy, Lucas Beyer, Alexander Kolesnikov, Dirk Weissenborn, Xiaohua Zhai, Thomas Unterthiner, Mostafa Dehghani, Matthias Minderer, Georg Heigold, Sylvain Gelly, et al. An image is worth 16x16 words: Transformers for image recognition at scale. *arXiv preprint arXiv:2010.11929*, 2020. 6
- [7] Chuang Gan, Yandong Li, Haoxiang Li, Chen Sun, and Boqing Gong. Vqs: Linking segmentations to questions and answers for supervised attention in vqa and question-focused semantic segmentation. In *Proceedings of the IEEE/CVF International Conference on Computer Vision*, pages 1811–1820, 2017. 3
- [8] Yash Goyal, Tejas Khot, Douglas Summers-Stay, Dhruv Batra, and Devi Parikh. Making the v in vqa matter: Elevating the role of image understanding in visual question answering. In *Proceedings of the IEEE/CVF Conference on Computer Vision and Pattern Recognition*, pages 6904–6913, 2017. 2
- [9] Danna Gurari, Qing Li, Abigale J Stangl, Anhong Guo, Chi Lin, Kristen Grauman, Jiebo Luo, and Jeffrey P Bigham. Vizwiz grand challenge: Answering visual questions from blind people. In *Proceedings of the IEEE/CVF Conference on Computer Vision and Pattern Recognition*, pages 3608–3617, 2018. 3
- [10] Kaiming He, Xiangyu Zhang, Shaoqing Ren, and Jian Sun. Deep residual learning for image recognition. In *Proceedings of the IEEE/CVF Conference on Computer Vision and Pattern Recognition*, pages 770–778, 2016. 5, 6
- [11] Yutao Hu, Tianbin Li, Quanfeng Lu, Wenqi Shao, Junjun He, Yu Qiao, and Ping Luo. Omnimedvqa: A new large-scale comprehensive evaluation benchmark for medical lvlm. In *Proceedings of the IEEE/CVF Conference on Computer Vision and Pattern Recognition*, pages 22170–22183, 2024. 2
- [12] Drew A Hudson and Christopher D Manning. Gqa: A new dataset for real-world visual reasoning and compositional question answering. In *Proceedings of the IEEE/CVF Conference on Computer Vision and Pattern Recognition*, pages 6700–6709, 2019. 3
- [13] Justin Johnson, Bharath Hariharan, Laurens Van Der Maaten, Li Fei-Fei, C Lawrence Zitnick, and Ross Girshick. Clevr: A diagnostic dataset for compositional language and elementary visual reasoning. In *Proceedings of the IEEE/CVF Conference on Computer Vision and Pattern Recognition*, pages 2901–2910, 2017. 2
- [14] Alexander Kirillov, Eric Mintun, Nikhila Ravi, Hanzi Mao, Chloe Rolland, Laura Gustafson, Tete Xiao, Spencer Whitehead, Alexander C Berg, Wan-Yen Lo, et al. Segment anything. In *Proceedings of the IEEE/CVF International Conference on Computer Vision*, pages 4015–4026, 2023. 6
- [15] Ranjay Krishna, Yuke Zhu, Oliver Groth, Justin Johnson, Kenji Hata, Joshua Kravitz, Stephanie Chen, Yannis Kalantidis, Li-Jia Li, David A Shamma, et al. Visual genome: Connecting language and vision using crowdsourced dense image annotations. *International Journal of Computer Vision*, 123:32–73, 2017. 2
- [16] Jie Lei, Licheng Yu, Tamara L Berg, and Mohit Bansal. Tvqa+: Spatio-temporal grounding for video question answering. *arXiv preprint arXiv:1904.11574*, 2019. 3
- [17] Ke Li, Di Wang, Haojie Xu, Haodi Zhong, and Cong Wang. Language-guided progressive attention for visual grounding in remote sensing images. *IEEE Transactions on Geoscience and Remote Sensing*, 2024. 3
- [18] Tsung-Yi Lin, Piotr Dollár, Ross Girshick, Kaiming He, Bharath Hariharan, and Serge Belongie. Feature pyramid networks for object detection. In *Proceedings of the IEEE/CVF Conference on Computer Vision and Pattern Recognition*, pages 2117–2125, 2017. 5
- [19] Sihan Liu, Yiwei Ma, Xiaoqing Zhang, Haowei Wang, Jiayi Ji, Xiaoshuai Sun, and Rongrong Ji. Rotated multi-scale interaction network for referring remote sensing image segmentation. In *Proceedings of the IEEE/CVF Conference on Computer Vision and Pattern Recognition*, pages 26658–26668, 2024. 3
- [20] Sylvain Lobry, Diego Marcos, Jesse Murray, and Devis Tuia. Rsvqa: Visual question answering for remote sensing data. *IEEE Transactions on Geoscience and Remote Sensing*, 58(12):8555–8566, 2020. 6, 7
- [21] Ilya Loshchilov and Frank Hutter. Decoupled weight decay regularization. *arXiv preprint arXiv:1711.05101*, 2017. 6
- [22] Jie Ma, Pinghui Wang, Dechen Kong, Zewei Wang, Jun Liu, Hongbin Pei, and Junzhou Zhao. Robust visual question answering: Datasets, methods, and future challenges. *IEEE Transactions on Pattern Analysis and Machine Intelligence*, 2024. 2
- [23] Alec Radford, Jong Wook Kim, Chris Hallacy, Aditya Ramesh, Gabriel Goh, Sandhini Agarwal, Girish Sastry, Amanda Askell, Pamela Mishkin, Jack Clark, et al. Learning transferable visual models from natural language super-

- vision. In *International Conference on Machine Learning*, pages 8748–8763. PMLR, 2021. 4, 6
- [24] Mengye Ren, Ryan Kiros, and Richard Zemel. Exploring models and data for image question answering. *Advances in Neural Information Processing Systems*, 28, 2015. 2
- [25] Marco Tulio Ribeiro, Sameer Singh, and Carlos Guestrin. ” why should i trust you?” explaining the predictions of any classifier. In *Proceedings of the 22nd ACM SIGKDD international conference on knowledge discovery and data mining*, pages 1135–1144, 2016. 3
- [26] Ramprasaath R Selvaraju, Michael Cogswell, Abhishek Das, Ramakrishna Vedantam, Devi Parikh, and Dhruv Batra. Grad-cam: Visual explanations from deep networks via gradient-based localization. In *Proceedings of the IEEE/CVF International Conference on Computer Vision*, pages 618–626, 2017. 3
- [27] Minseok Seo, Hakjin Lee, Yongjin Jeon, and Junghoon Seo. Self-pair: Synthesizing changes from single source for object change detection in remote sensing imagery. In *Proceedings of the IEEE/CVF Winter Conference on Applications of Computer Vision*, pages 6374–6383, 2023. 1
- [28] Jiajin Tang, Ge Zheng, Cheng Shi, and Sibe Yang. Contrastive grouping with transformer for referring image segmentation. In *Proceedings of the IEEE/CVF Conference on Computer Vision and Pattern Recognition*, pages 23570–23580, 2023. 6, 7
- [29] Shiqi Tian, Ailong Ma, Zhuo Zheng, and Yanfei Zhong. Hi-ucd: A large-scale dataset for urban semantic change detection in remote sensing imagery. *arXiv preprint arXiv:2011.03247*, 2020. 2, 3
- [30] Aysim Toker, Lukas Kondmann, Mark Weber, Marvin Eisenberger, Andrés Camero, Jingliang Hu, Ariadna Pregel Hoderlein, Çağlar Şenarar, Timothy Davis, Daniel Cremers, et al. Dynamicearthnet: Daily multi-spectral satellite dataset for semantic change segmentation. In *Proceedings of the IEEE/CVF Conference on Computer Vision and Pattern Recognition*, pages 21158–21167, 2022. 2
- [31] Aisha Urooj, Hilde Kuehne, Kevin Duarte, Chuang Gan, Niels Lobo, and Mubarak Shah. Found a reason for me? weakly-supervised grounded visual question answering using capsules. In *Proceedings of the IEEE/CVF Conference on Computer Vision and Pattern Recognition*, pages 8465–8474, 2021. 3
- [32] Di Wang, Fuyu Dong, Ke Li, and Duo Chen. Kernel-adaptive change detection network in remote sensing imagery. In *IEEE International Geoscience and Remote Sensing Symposium*, pages 10192–10196. IEEE, 2024. 1, 6
- [33] Junjue Wang, Zhuo Zheng, Zihang Chen, Ailong Ma, and Yanfei Zhong. Earthvqa: Towards queryable earth via relational reasoning-based remote sensing visual question answering. In *Proceedings of the AAAI Conference on Artificial Intelligence*, pages 5481–5489, 2024. 2, 6, 7
- [34] Zhaoqing Wang, Yu Lu, Qiang Li, Xunqiang Tao, Yandong Guo, Mingming Gong, and Tongliang Liu. Cris: Clip-driven referring image segmentation. In *Proceedings of the IEEE/CVF Conference on Computer Vision and Pattern Recognition*, pages 11686–11695, 2022. 6, 7
- [35] Chen Wu, Bo Du, and Liangpei Zhang. Fully convolutional change detection framework with generative adversarial network for unsupervised, weakly supervised and regional supervised change detection. *IEEE Transactions on Pattern Analysis and Machine Intelligence*, 45(8):9774–9788, 2023. 2
- [36] Zunnan Xu, Zhihong Chen, Yong Zhang, Yibing Song, Xiang Wan, and Guanbin Li. Bridging vision and language encoders: Parameter-efficient tuning for referring image segmentation. In *Proceedings of the IEEE/CVF International Conference on Computer Vision*, pages 17503–17512, 2023. 3, 6, 7
- [37] Kunping Yang, Gui-Song Xia, Zicheng Liu, Bo Du, Wen Yang, Marcello Pelillo, and Liangpei Zhang. Asymmetric siamese networks for semantic change detection in aerial images. *IEEE Transactions on Geoscience and Remote Sensing*, 60:1–18, 2021. 2, 3
- [38] Li Yang, Yan Xu, Chunfeng Yuan, Wei Liu, Bing Li, and Weiming Hu. Improving visual grounding with visual-linguistic verification and iterative reasoning. In *Proceedings of the IEEE/CVF Conference on Computer Vision and Pattern Recognition*, pages 9499–9508, 2022. 3
- [39] Zhao Yang, Jiaqi Wang, Yansong Tang, Kai Chen, Hengshuang Zhao, and Philip HS Torr. Lavt: Language-aware vision transformer for referring image segmentation. In *Proceedings of the IEEE/CVF Conference on Computer Vision and Pattern Recognition*, pages 18155–18165, 2022. 3, 6, 7
- [40] Jiabo Ye, Junfeng Tian, Ming Yan, Xiaoshan Yang, Xuwu Wang, Ji Zhang, Liang He, and Xin Lin. Shifting more attention to visual backbone: Query-modulated refinement networks for end-to-end visual grounding. In *Proceedings of the IEEE/CVF Conference on Computer Vision and Pattern Recognition*, pages 15502–15512, 2022. 3
- [41] Zhenghang Yuan, Lichao Mou, Zhitong Xiong, and Xiao Xi-zhu. Change detection meets visual question answering. *IEEE Transactions on Geoscience and Remote Sensing*, 60: 1–13, 2022. 1, 2, 6, 7
- [42] Zhuo Zheng, Ailong Ma, Liangpei Zhang, and Yanfei Zhong. Change is everywhere: Single-temporal supervised object change detection in remote sensing imagery. In *Proceedings of the IEEE/CVF International Conference on Computer Vision*, pages 15193–15202, 2021. 1
- [43] Zhuo Zheng, Yanfei Zhong, Shiqi Tian, Ailong Ma, and Liangpei Zhang. Changemask: Deep multi-task encoder-transformer-decoder architecture for semantic change detection. *ISPRS Journal of Photogrammetry and Remote Sensing*, 183:228–239, 2022. 2
- [44] Zhuo Zheng, Shiqi Tian, Ailong Ma, Liangpei Zhang, and Yanfei Zhong. Scalable multi-temporal remote sensing change data generation via simulating stochastic change process. In *Proceedings of the IEEE/CVF International Conference on Computer Vision*, pages 21818–21827, 2023. 1
- [45] Yuke Zhu, Oliver Groth, Michael Bernstein, and Li Fei-Fei. Visual7w: Grounded question answering in images. In *Proceedings of the IEEE/CVF Conference on Computer Vision and Pattern Recognition*, pages 4995–5004, 2016. 3